ACS Catalysis

Research Article

pubs.acs.org/acscatalysis

Organometallic Ruthenium Nanoparticles as Model Catalysts for CO Hydrogenation: A Nuclear Magnetic Resonance and Ambient-Pressure X-ray Photoelectron Spectroscopy Study

Luis M. Martínez-Prieto,[†,‡] Sophie Carenco,[§] Cheng H. Wu,[∥] Eric Bonnefille,[†,‡] Stephanus Axnanda,[⊥] Zhi Liu,[⊥] Pier F. Fazzini,[@] Karine Philippot,[†,‡] Miquel Salmeron,*[,∥,#] and Bruno Chaudret*[,@]

[†]Laboratoire de Chimie de Coordination, CNRS, LCC, 205, Route de Narbonne, F-31077 Toulouse, France

[‡]Université de Toulouse, UPS, INPT, LCC, 31077 Toulouse, France

[§]Chemical Sciences Division, Lawrence Berkeley National Laboratory, Berkeley, California 94720-8176, United States

[∥]Materials Sciences Division, Lawrence Berkeley National Laboratory, Berkeley, California 94720, United States

[⊥]Advanced Light Source, Lawrence Berkeley National Laboratory, Berkeley, California 94720, United States

[@]LPCNO, Laboratoire de Physique et Chimie des Nano-Objets, UMR5215 INSA-CNRS-UPS, Institut des Sciences appliquées, 135, Avenue de Rangueil, F-31077 Toulouse, France

[#]Department of Materials Science & Engineering, University of California, Berkeley, California 94720, United States

Supporting Information

ABSTRACT: We present a study of the structure and reactivity of Ru nanoparticles of different sizes (1.3, 1.9, and 3.1 nm) for CO hydrogenation using gas-phase nuclear magnetic resonance and mass spectroscopy. In addition, the nanoparticles were characterized under reaction mixtures *in situ* by ambient-pressure X-ray photoelectron spectroscopy. We found that during reaction the Ru is in the metallic state and that the diphosphine ligands [bis(diphenylphosphino)butane (dppb)] on the surface of 1.9 and 3.1 nm nanoparticles not only act as capping and protecting agents but also stay on the surface during reaction and improve their activity and selectivity toward C_2−C_4 hydrocarbons.

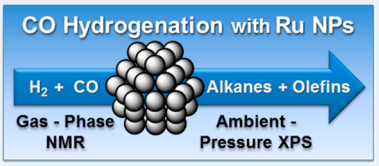

KEYWORDS: *ruthenium nanoparticles, model Fischer−Tropsch synthesis, surface chemistry, ligand effect, ambient-pressure XPS, NMR, FTIR, mass spectrometry*

INTRODUCTION

Fischer−Trospch synthesis (FTS) has generated renewed interest because it provides sulfur- and nitrogen-free fuels from abundant raw sources of carbon and oxygen (natural gas, coal, and biomass).[1,2] The design of novel catalysts with high activity at low temperature and selectivity toward long-chain hydrocarbons is one of the important challenges of contemporary FTS.[3,4] Iron and cobalt catalysts are preferable for economic reasons,[5−8] while ruthenium is usually known as the most active metal working at the lowest temperature.[5,9−11] Recent studies have demonstrated the potential of ruthenium nanoparticles (Ru NPs) to achieve CO conversion under a range of experimental conditions.[12−19] In addition, it has recently been shown that Ru nanocatalysts exhibit size dependence in activity but not in selectivity, for both CO reduction and CO oxidation reactions.[20,21] Typical nanocatalysts are in general prepared by impregnation, where a Ru salt is deposited on a large-surface area support (silica, titanium dioxide, etc.) and reduced to produce the active species. Under these conditions, a distribution of metallic Ru NPs of various sizes and shapes is generally obtained. Most often, surfactants are used to improve the dispersion of Ru NPs on the support and to narrow the size distribution,[22] although they should be eliminated (by washing or burning) prior to the catalytic reaction to liberate surface active sites. Colloidal Ru NPs require stabilizers that may have a steric or electronic effect and that can modulate the size and the shape of the nanoparticles.[21,23−26] A recent study shows that a strong ligand such as a thiol can modify the activity and selectivity of Ru NPs in FTS, whereas steric or second-sphere stabilizers will play only on the accessibility of the metal center.[27]

We report in this study that under mild reaction conditions diphosphine ligands can improve the selectivity of small Ru NPs while keeping a sufficient activity in CO hydrogenation conducted at low temperatures (120 and 150 °C). This reaction is a model for understanding FTS on the catalysts and, in particular, its first stages (CO dissociation and initiation of chain growth). Our results also evidence that the ligand effects are due to a surface modification of the nanocatalyst, by comparing the catalytic activity of two samples of Ru NPs with the same ligand shell but two different sizes (3.1 and 1.9 nm). Nuclear magnetic resonance (NMR) spectroscopy was used to

Received: July 22, 2014
Revised: August 3, 2014
Published: August 5, 2014

   dx.doi.org/10.1021/cs5010536 | ACS Catal. 2014, 4, 3160−3168

characterize the surface chemistry of the Ru NPs as well as the chemical state of the dppb ligands. In parallel experiments using ambient-pressure X-ray photoelectron spectroscopy (APXPS), we found that the phosphorus ligands remain on the surface of the Ru NPs under reaction conditions, although their structure was affected. This work provides new insights into the chemical structure of ligand-caped Ru nanocatalysts and highlights the interest in such systems in terms of FTS activity and selectivity.

RESULTS

Synthesis and Characterization of Nanoparticles. Traditional preparation routes for Ru nanocatalysts for FTS involve the deposition of Ru(III) species (typically salts) on a support followed by their reduction under dihydrogen to form Ru(0) NPs.[15,28,29] In contrast with this, our strategy for studying CO hydrogenation was to use Ru(0) NPs directly protected by a polymer [polyvinylpyrrolidone (PVP)][30] or a diphosphine ligand [bis(diphenylphosphino)butane (dppb)].[31] The NPs had a small diameter (<10 nm), a limited size distribution, and good dispersion on the support. PVP provides steric stabilization and is used in large excess, while dppb is a σ-donor and a weak π-acceptor bidendate ligand that is known to strongly coordinate to the surface.[31] Because recent reports suggest that slightly larger NPs can be beneficial for FTS activity and selectivity for longer hydrocarbons,[12,20,32] we looked for a method for preparing larger nanoparticles containing the same ligand. Because it was not possible to grow directly larger Ru-dppb NPs in one step, we synthesized Ru NPs by a two-step procedure (*vide infra*), which allowed us to have larger Ru NPs exhibiting the same capping ligand (dppb).

The Ru NPs were prepared by hydrogenating at room temperature (r.t.) the organometallic precursor [Ru(cod)(cot)] (cod, 1,5-cyclooctadiene; cot, 1,3,5-cyclooctatriene) under H_2 (3 bar) in a tetrahydrofuran solution and in the presence of the PVP polymer or the dppb ligand.[31] These samples were named Ru-PVP and Ru-dppb, respectively. The Ru cores display a hcp structure in both cases, with diameters of 1.3(0.2) and 1.9(0.4) nm for Ru-PVP and Ru-dppb, respectively (Figure 1a,b). For such small sizes, important modifications in the electronic configuration of the particles are expected.[33] These Ru NPs are known to be active in reactions such as hydrogenation of styrene under mild conditions (25 °C, 3 bar of H_2)[34] and to adsorb CO molecules alongside the existing ligands.[35]

The third sample of Ru NPs was synthesized following a two-step route. First, weakly stabilized Ru NPs were prepared by decomposition of [Ru(cod)(cot)] under H_2 (3 bar) in heptanol according to a previously reported procedure,[36] and second, a ligand exchange was performed to introduce dppb onto the surface of the nanoparticles (Figure 2a). Heptanol was selected because, as demonstrated previously, it can provide monodisperse crystalline NPs (~3 nm), hereafter named Ru-hept.[36] Given that heptanol is weakly coordinated at the Ru surface, partial ligand exchange could be performed at room temperature by addition of 0.1 equiv of dppb to Ru-hept NPs in a 1:1 heptanol/tetrahydrofuran (THF) mixture. This resulted in the formation of 3.1(0.4) nm dppb-covered Ru NPs (Figure 1c), hereafter named Ru-hept-dppb. As expected, these new Ru NPs exhibit the same mean size as the parent Ru-hept NPs but display at their surface coordinated dppb ligands (*vide infra*). High-resolution transmission electron microscopy (HRTEM) images show that there is a coexistence of irregularly shaped polycrystalline and monocrystalline particles (Figure 3), similar to that of the Ru-hept NPs used initially. No considerable structural differences could be observed between Ru-hept and

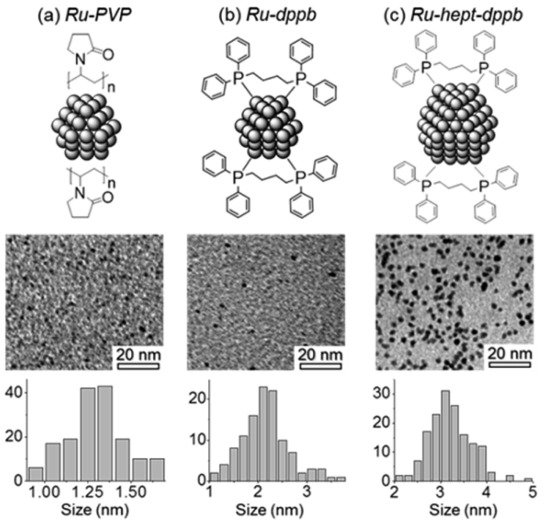

Figure 1. Schematic structure, TEM images, and size distributions of three Ru(0) NPs samples: Ru-PVP (a), Ru-dppb (b), and Ru-hept-dppb (c).

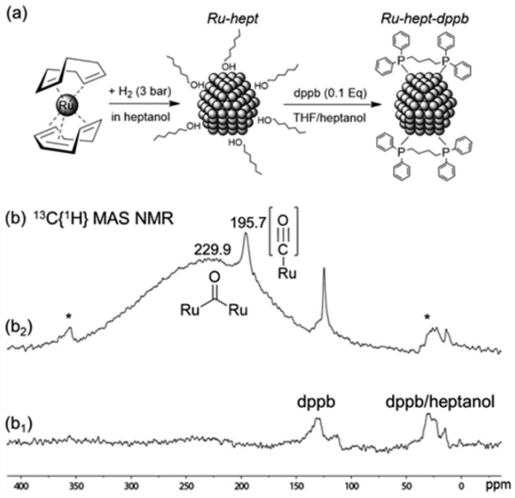

Figure 2. (a) Two-step route followed for the synthesis of Ru-hept-dppb NPs. (b_1) Solid state ^{13}C MAS NMR spectrum of Ru-hept-dppb NPs as prepared. (b_2) Solid state $^{13}C\{^1H\}$ MAS NMR spectrum of Ru-hept-dppb NPs after reaction with ^{13}CO (0.6 bar, 20 h, r.t.).

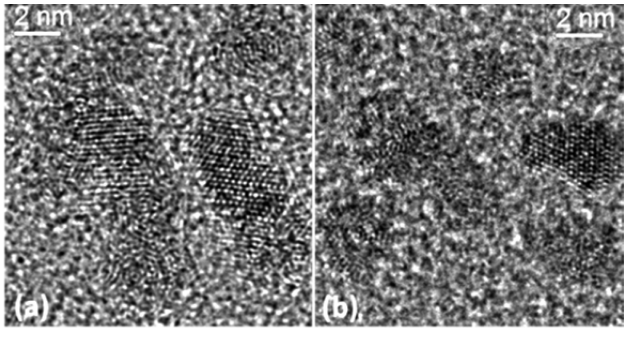

Figure 3. HRTEM images of Ru-hept-dppb (a) and Ru-hept (b) NPs.

dx.doi.org/10.1021/cs5010536 | ACS Catal. 2014, 4, 3160−3168

Table 1. FTS Activities[a] and Selectivities[b] of Ru NPs as a Function of the Stabilizer, Size, and Reaction Temperature

Entry (lines)	Catalyst and mean diameter in nm	Activity: H_2 consumed (%) *TOF (s^{-1})*			Selectivity (%) *for methane, alkanes and alkenes (C_2-C_4)*
		5 days		1 day	
		120°C	150°C	150°C	
1	*Ru-PVP*	0	7.8	-	
	1.3 (0.2)	0	$8.3\cdot10^{-7}$	-	
2	*Ru-dppb*	29.7	100	85.2	
	1.9 (0.4)	$1.4\cdot10^{-6}$	-	$2.0\cdot10^{-5}$	
3	*Ru-hept-dppb*	16.4	100	31.9	
	3.1 (0.4)	$1.3\cdot10^{-6}$	-	$1.3\cdot10^{-5}$	
Entry (columns) →		a	b	C	

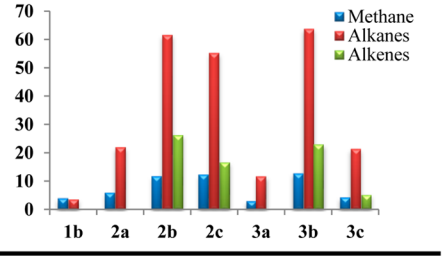

[a]Activity evaluated from the consumption of H_2. TOFs normalized per number of Ru surface atoms. [b]Selectivity calculated only for methane, alkanes, and alkenes as products (water and remaining H_2 and CO omitted for the sake of clarity). Values listed in Table S1 of the Supporting Information.

Ru-hept-dppb. Fourier analysis of the HRTEM images confirmed that the Ru NPs retain the hcp structure of bulk Ru (Figure S1 of the Supporting Information). HRTEM observations performed on different specimens also show that the largest particles are polycrystalline and that the size of the average monocrystalline domain is compatible with the coherence length measured via WAXS [wide-angle X-ray scattering (Figure S2 of the Supporting Information)].

We also performed studies using $^{13}C\{^1H\}$ MAS NMR that evidenced the presence of dppb (Figure $2b_1$), as shown by the series of peaks corresponding to alkyl and aryl carbons at δ 25 and 130, respectively. $^{31}P\{^1H\}$ NMR showed a peak at δ 34.5, confirming the coordination of dppb on the surface of NPs (Figure S3 of the Supporting Information). This signal is slightly shifted to a low field compared to dppb coordinated on the Ru-dppb nanoparticles (δ 25). Heptanol could not be clearly identified on the NPs by ^{13}C MAS NMR as the corresponding peak at ∼25 ppm overlaps with those of the dppb alkyl chain, although a small amount was detected by XPS alongside the phosphorus-containing ligands.

CO adsorption has been previously used as a probe to identify the available surface sites and their location on the nanoparticles following characterization by infrared and solid state NMR spectroscopy. For this purpose, ^{13}CO was added to Ru-hept and characterized by ^{13}C MAS NMR. A strong signal is present at 245 ppm [$w_{1/2}$ = 1650 Hz (Figure S4 of the Supporting Information)] with an additional peak at 184 ppm that may arise from multicarbonyl sites at apex locations of the particle. The chemical shift of the main signal corresponds to bridging CO ligands, and the low intensity of the spinning side bands is in agreement with the mobility of CO on the surface of the NPs. The same reaction was conducted with Ru-hept-dppb and monitored by ^{13}C MAS NMR. Figure $2b_2$ shows the ^{13}C MAS NMR spectrum of Ru-hept-dppb after reaction for 20 h with 0.6 bar of ^{13}CO at r.t. It shows a sharp peak at δ 195.7 displaying spinning side bands (asterisk) that can be attributed to terminal CO ligands, and an intense and very broad resonance centered near 230 ppm ($w_{1/2}$ = 3100 Hz) that can be attributed to bridging CO groups.[35,37]

^{13}C CP MAS NMR (Figure S8 of the Supporting Information) shows that the intensity of bridging CO decreases in comparison with the terminal ones, because of the substitution of CO groups with dppb ligands. The signal is broader than that for Ru-hept (after exposure to ^{13}CO) as a result of reduced mobility and a greater diversity of chemical environments. In addition, a CP MAS experiment evidenced the presence of terminal CO groups located near the phosphine ligands, i.e., near apexes.

The presence of terminal and bridging CO signals is reminiscent of the spectrum of Ru-dppb upon reaction with ^{13}CO and suggests the absence of fluxionality of CO on the surface of the particles at r.t. and in the solid state.[35] The half-height width of the signal is much larger than in Ru-dppb and Ru-hept, suggesting a diversity of sites in addition to the low mobility of the CO ligands, in agreement with the presence of dppb on Ru-hept-dppb as well as the existence of extended faces allowing the coordination of CO in bridge sites.

Reactivity Studies. One open question of heterogeneous catalysis and specifically of FTS is the role of organic ligands and the catalytic activity and selectivity. We studied this effect on the CO reduction reaction (dissociation and subsequent growth of alkane chains): the activity and selectivity of Ru-PVP, Ru-dppb, and Ru-hept-dppb NP powders [∼0.02−0.05 mmol of Ru(0)] were evaluated under mild reaction conditions, at temperatures of 150 and 120 °C, and a total syngas pressure of 3 bar (1:1 molar mixture of H_2 and CO). The reactions were conducted in batch mode using 2 mL quick pressure valve NMR tubes as small-scale reactors and ^{13}C isotope-enriched carbon monoxide, which allowed us to follow easily the formation of products by gas-phase NMR. Mass spectrometry (MS) was complementarily used to confirm the nature of the products formed. For all reactions, the absence of high-mass products (C_5 and higher) was checked by gas chromatography (GC) after addition of anisole in the NMR tube to collect any liquid product. As expected given that the pressure and temperature used in our study are relatively low, the anisole fractions did not show any significant content of long-chain alkanes or alkenes.[38]

Under the same reaction conditions (120 or 150 °C, 5 days), the Ru-PVP and Ru-dppb NPs presented very different activities. At 120 °C, Ru-PVP showed no activity (Table 1, entry 1a) while Ru-dppb (Table 1, entry 2a) converted around 30% of H_2 to form water byproduct, and C_1−C_4 alkanes as main carbon-containing products (Table 1, right). An increase in the temperature to 150 °C resulted in a small conversion of H_2 (7.8%) into methane and alkanes on the Ru-PVP, confirming the poor activity of this catalyst for FTS at low temperatures (Table 1, entry 1b). In contrast, Ru-dppb converted all the H_2 into C_2−C_4 alkanes (61%), alkenes (26%), and methane (12%) (Table 1, entry 2b).

dx.doi.org/10.1021/cs5010536 | ACS Catal. 2014, 4, 3160−3168

In addition, benzene (identified by a singlet at 7.4 ppm in ^{1}H gas-phase spectra) was observed in the products of reactions on Ru-dppb (Table 1, reaction 2) in small amounts (~3%) which was not taken into account in the selectivity calculation. Because the formation of benzene was also observed on Ru-hept-dppb and on dppb-containing samples, it is likely the result of partial dppb decomposition (breaking of the P−Ph bonds) rather than FTS. Similarly, for Ru-PVP, some PVP decomposition was also observed as shown by the extra peaks in the alkane region, at 1.8 and 1.0 ppm.

To determine the turnover frequency (TOF), the reaction was performed for 1 day (Table 1, 2c), to ensure that the Ru-dppb had converted most of the H_2 (85.2%), with a product selectivity similar to that of a majority of C_2−C_4 alkanes (63.1%).

From the first set of experiments (Table 1, entries 1 and 2), the following conclusions can be drawn. First, even under the mild conditions applied, differences between the nanocatalysts are observed. While the TOF is low, the onset of the catalytic reaction occurs at different temperatures depending on the sample, namely, 150 °C for Ru-PVP and 120 °C for Ru-dppb. This difference can be related either to the presence of surface ligands or to the difference in the size of the NPs. The TOF estimated from the batch reactions was 24 times larger for Ru-dppb than for Ru-PVP at 150 °C, and Ru-dppb was even more active at 120 °C than Ru-PVP at 150 °C. The precise role of dppb is still unclear. From NMR studies, we know that dppb is coordinated and that it impedes the mobility of CO on the surface of the particles. Two possible effects can be present: an electronic effect arising from the presence of phosphorus-containing donor ligands (though this effect is expected to be weak because the electron density will be diluted over the whole nanoparticle) or a combined steric/electronic effect resulting from the presence on the dppb-stabilized nanoparticles of sites allowing hydride coordination associated with a lower density of surface CO groups and therefore a lower level of deactivation of the ruthenium surface by CO.

It is noteworthy that under these mild conditions all catalysts produced mostly methane and light alkanes instead of liquid fuels, as shown by the quasi-absence of C_4 species and the absence of chains of C_5 and higher. Furthermore, Ru-dppb showed a selectivity (85.3%) higher than that of Ru-PVP for C_2−C_4 alkanes and alkenes versus methane (47.4%) at 150 °C. This observation is of interest with regard to the selectivity in CO hydrogenation and the fact that ruthenium is often described as producing mostly methane.[20]

To distinguish between size and ligand effects on the reactivity of the NPs, we conducted CO hydrogenation reactions with Ru-hept-dppb samples prepared with the same ligands but different sizes using the same experimental conditions that were used for Ru-PVP and Ru-dppb (Table 1, entry 3). At 120 °C, the Ru-hept-dppb NPs presented an activity comparable to that of Ru-dppb, with TOFs on the same order of magnitude. A very similar selectivity was observed also, with mostly C_2−C_4 alkanes as products. When the temperature was increased to 150 °C, an increased activity was observed with a full consumption of H_2 in 5 days (Table 1, entry 3b). The same reaction conducted for 1 day only (Table 1, entry 3c) resulted in a level of H_2 conversion (31.9%) lower than that with Ru-dppb (85.2%), although again the TOFs were in the same range (1.3×10^{-5} s^{-1} vs 2.0×10^{-5} s^{-1}). Accordingly, the selectivity of Ru-hept-dppb matched well that of Ru-dppb. This means either that there is no size effect or that there are compensated size and other (steric/electronic) effects on the particle. It is noteworthy that a difference in activity between ruthenium nanoparticles accommodating either hydrogenated or nonhydrogenated aryl-phosphines has been described by some of us.[39,40] A similar effect that again may involve steric effects of the more bulky hydrogenated phosphine and an electronic effect related to the π-stacking of the phenyl groups could be present.

This study demonstrates that the capping agent plays a critical in the nanocatalyst performance, with dppb giving rise to Ru NPs more active than those for PVP while still ensuring good stability. This was shown by "post-mortem" analysis of the NPs by TEM after reaction for 5 days at 150 °C in which weak broadening of the size distribution was observed, but without a significant change in the mean size, confirming that there was no sintering during the reaction (Figure S11 of the Supporting Information). Thus, after reaction 2b in Table 1, which left excess CO, reloading the reactor with 3 bar of H_2 allowed further reaction leading after an additional 5 days at 150 °C to consumption of all CO and formation of additional alkanes and methane. This is a good indication that any modification of the dppb ligands in the course of the first run did not affect significantly the activity of the catalyst over time. Interestingly, this second step performed with a H_2-rich gas phase also resulted in the full hydrogenation of the alkenes formed in the first step, pointing out that, under these conditions, the classical activity of Ru NPs in hydrogenation was preserved. With regard to NMR characterization after catalysis, ^{31}P NMR spectra (Figure S6 of the Supporting Information) evidence some decoordination of the phosphine ligands (signals near 0 ppm) as well as some hydrogenation of the phosphine arene rings (shift from ~35 to 64 ppm) but no dramatic collapse of the peaks. For the ^{13}C NMR spectra, the only important changes concern an additional terminal CO signal at 184 ppm, probably associated with the presence of nearby hydrogenated phosphines that are visible on the spectrum near 30 ppm, in agreement with ^{31}P NMR observations.

An interesting observation in these systems is that although Ru CO hydrogenation catalysts are considered to be insensitive to the particle size from the point of view of selectivity,[20,28] strong differences in the selectivity toward methane were observed when using Ru-PVP or Ru-dppb. Previous studies suggest that bulky ligands would bind first to the most accessible atoms, i.e., those at the apex, and hence inhibit their catalytic properties.[34] Our results therefore suggest that apex and face atoms display different reactivity that could be modulated by the use of ligands.

XPS Studies. To understand the nature of the active surface exposed to syngas and the role of the ligands, we also analyzed Ru-dppb NPs by ambient-pressure X-ray photoelectron spectroscopy (APXPS), which makes it possible to collect spectra in the presence of a gas phase at pressures of a few torr.[41,42] Although this pressure is 3 orders of magnitude below the nominal reaction pressure, it is high enough to ensure that the surface is saturated with adsorbed species as expected to be the case under pressures of ≥1 bar.[43−49] In these studies, the samples were prepared by drop-casting a colloidal THF solution of nanoparticles on a gold foil. After their introduction into the measurement chamber, they were exposed to mixtures of CO and H_2 and heated to 150 °C. We present only the data obtained for Ru-dppb NPs below, with the Ru-hept-dppb NPs exhibiting a similar behavior. The binding energy (BE) scale

dx.doi.org/10.1021/cs5010536 | ACS Catal. 2014, 4, 3160−3168

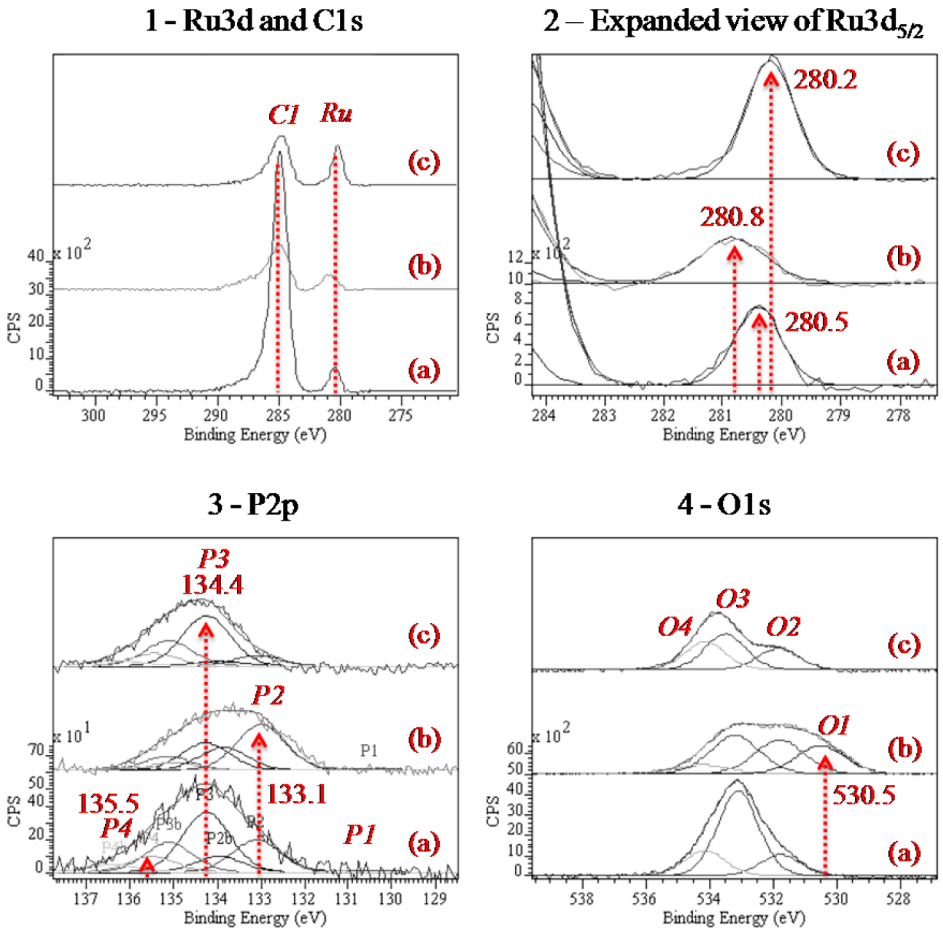

Figure 4. Ambient-pressure XPS of Ru-dppb NPs (a) after synthesis, (b) after oxidation in O_2 at 250 °C, and (c) after reduction in H_2 at 250 °C. The energy scale is calibrated using the Au 4f binding energy of 84.0 eV and the Fermi edge at 0.0 eV. Spectra are displayed after background subtraction. The *Y* axis scale is counts per second.

was calibrated by fixing the Au 4f peak at 84.0 eV and the Fermi level edge at 0 eV.

Initial State of Ru-dppb NPs. Before reaction, the C 1s spectrum showed a main asymmetric component at a binding energy (BE) of 284.8 eV (named C1), corresponding to CH_x moieties in the organic ligands (Figure 4, spectrum 1a, and Figure S9 of the Supporting Information). The small peak at a higher BE (named C3 at 287.9 eV in Figure S9 of the Supporting Information) was attributed to residual THF from the sample preparation step. In the same region, the Ru 3d components can be observed. In particular, there is a Ru $3d_{3/2}$ peak buried under the main C 1s peak (named Ru_b in Figure S9 of the Supporting Information), and the Ru $3d_{5/2}$ peak (named Ru on all spectra) at a BE of 280.5 eV, slightly different from the reported value of 280.0 eV of metallic Ru.[50] However, the O 1s spectrum did not indicate the presence of RuO_x, which would produce a peak at 529.5 eV (Figure S9 of the Supporting Information).[51] The higher BE observed for Ru $3d_{5/2}$ is likely due to the π-acceptor character of the dppb ligand coordinated to surface Ru atoms, and possibly to electronic effects due to the small size of the NPs, as was recently reported for Pt NPs.[33]

High-BE oxygen species were observed (Figure S9 of the Supporting Information), with a broad peak centered at 533.1 eV that can be decomposed into three components: O2 at 531.8 eV, O3 at 533.1 eV, and O4 at 534.2 eV. The main component, O3, was attributed to THF molecules and other oxygen species such as hydroxyl groups on the sample surface.

In the phosphorus 2p region, a broad peak was observed centered at 134.4 eV (Figure 4, spectrum 3a). No unbound dppb was observed at ~130 eV (P1 in Figure 4, spectrum 3a).[52] The P 2p peak was composed of three P 2p doublets (P $2p_{3/2}$ components were numbered from 2 to 4, and corresponding P $2p_{1/2}$ components were indexed with a subscript b): P2 at 133.1 eV, P3 at 134.4 eV, and P4 at 135.5 eV. P3 is attributed to dppb bound to the surface and P2 to noncoordinated dppb-oxidized species present as a minority species. P4 species were also observed in very small amounts and, considering their high BE, should correspond to P(+V) species (see Table S2 of the Supporting Information for the fitting procedure). These minority species were not clearly observed by ^{31}P NMR, probably because of the broadness of the dominant peak corresponding to coordinated dppb (Figure S7 of the Supporting Information), although the spectrum presented a small shoulder at low chemical shifts.

Ru-dppb NPs after Oxidation and Reduction. The proposed assignments were confirmed by a preliminary experiment in which the nanoparticles were oxidized under O_2 (500 mTorr) at 250 °C (Figure 4, spectra b). Such a treatment can remove the carbon part of the ligands, as shown by the decrease of the magnitude of the C 1s peak compared with that of the Ru $3d_{5/2}$ peak (Ru). As expected, Ru shifted to a higher BE (280.8 eV), and oxide peak O1 appeared at 530.5 eV in the O 1s region. Interestingly, the phosphorus was less affected by this oxidation than carbon: most of it (~90% of P)

dx.doi.org/10.1021/cs5010536 | ACS Catal. 2014, 4, 3160−3168

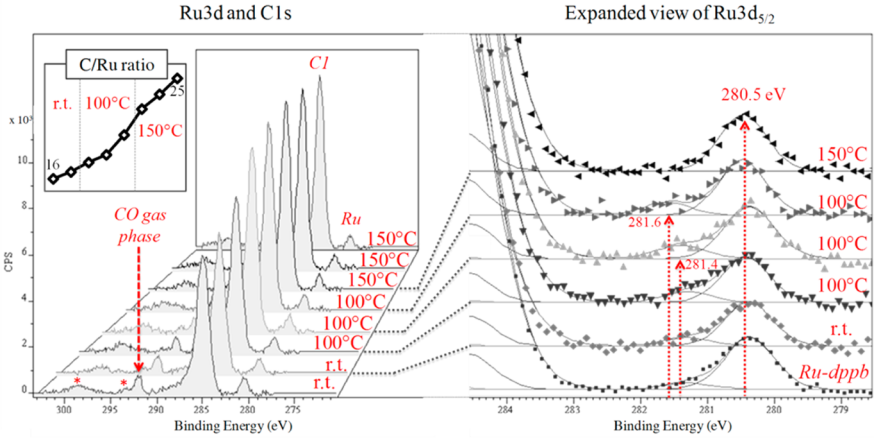

Figure 5. Ambient-pressure XPS of Ru-dppb NPs exposed to 450 mTorr of CO and 50 mTorr of H_2 at 150 °C. The left panel shows an overview of the C 1s and Ru 3d region. Ru is the Ru $3d_{5/2}$ peak. The inset shows the relative evolution of the C:Ru ratio (*Y*-axis) with temperature (*X*-axis). Asterisks denote inelastic losses of the main XPS peak. The right panel shows an expanded view of the Ru $3d_{5/2}$ region. Spectra are displayed after background subtraction. The *Y*-axis scale is counts per second.

stayed on the surface, although its bonding structure changed. As expected, the magnitude of peak P2, which we attribute to traces of phosphine oxide, increased.

The NPs were then reduced under H_2 (500 mTorr, 250 °C). A significant amount of phosphorus (~40%) disappeared as shown by the peaks in the P2 region. Interestingly, no detectable ruthenium phosphide was formed (no peak in the P1 region).[53] As expected, a reduction of the metal occurred, resulting in a lower BE peak (280.2 eV) that is very close to that of metallic ruthenium (Figure 4, spectrum 2c). This is consistent with our assumption that the relatively higher initial BE of Ru in Ru-dppb NPs is related to the ligand coordination.

Ru-dppb NPs Exposed to Model FTS Conditions. Fresh Ru-dppb nanoparticles were characterized in the presence of a Fischer–Tropsch reaction mixture consisting of 450 mTorr of CO and 50 mTorr of H_2 at 150 °C. A CO-rich mixture was selected here to decrease the reaction rate and maximize the chances to observe carbon-containing adsorbed species. APXPS revealed that, upon heating, the magnitude of the carbon C1 peak increased, indicating the formation of CH_x species and/or amorphous carbon as a consequence of the Fischer–Tropsch reaction (Figure 5, left and inset). This was consistent with the post-mortem $^{13}C\{^1H\}$ MAS NMR observations after a 5 day reaction at 150 °C (Figure S5 of the Supporting Information), showing the presence of carbonyl bridging (228 ppm) and terminal (191 ppm for monocarbonyl and 184 ppm for multicarbonyl) species, along with -CH_3 and -CH_2 groups from adsorbed alkanes and alkenes (both the products and ligands) at 14 and 29 ppm, respectively.

The main Ru peak did not undergo a change in position (Figure 5 right). However, an additional Ru component was observed at a higher BE under moderate heating (100 °C), indicative of a progressive oxidation of Ru under syngas.[54] We attribute this to the formation of surface oxide species as a result of CO dissociation.[55,56] However, as the temperature was increased to 150 °C, the oxide was reduced, giving back a metallic surface similar to that in the starting NPs. This observation of a temperature-dependent Ru oxidation state is in agreement with the observed catalytic activity that is much lower at 120 °C than at 150 °C. It is well-established that Ru should be metallic to act as a CO hydrogenation catalyst.[5] At lower temperatures, the Ru NPs cannot efficiently eliminate oxygen-containing species, while at higher temperatures, the formation of water from adsorbed H and O is more efficient. This could explain the size effect on activity for the parent reaction of FTS, as reported in other works,[20,32] because larger Ru-hept-dppb NPs underwent reduction at a lower temperature of 100 °C (Figure S11 of the Supporting Information).

The phosphorus 2p region reveals the changes in the dppb ligand headgroups during FTS reaction. As shown in Figure 6,

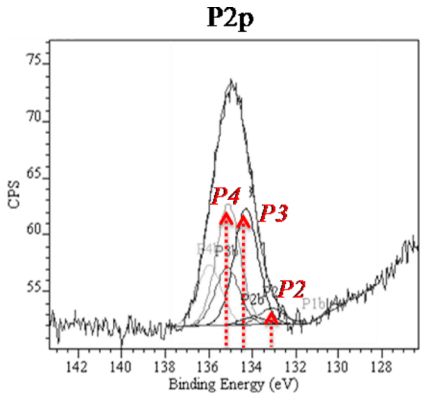

Figure 6. Ambient-pressure XPS in the P regions of Ru-dppb NPs after the Fischer–Tropsch reaction.

the peak components correspond to the same P-containing species as initially observed, but their relative ratios had changed. In particular, the P4 component grew by a factor ~4, which was accompanied by a similar growth of the O4 component (Figure S10 of the Supporting Information). We propose that these peaks correspond to P(+V) species, such as phosphonates [O═PR(OR)$_2$] or phosphates [O═P(OR)$_3$]. This attribution is consistent with the appearance of a new peak at 5.4 ppm on the post-mortem ^{31}P MAS NMR spectrum, which could also be due to phosphonates or phosphates (Figure S6 of the Supporting Information).

The mechanism of formation of these species is still unclear. It should be linked to the possible formation of adsorbed oxygen on the Ru NPs surface as a consequence of CO dissociation and the breaking of P–Ph bonds, as was observed by mass spectroscopy through the formation of benzene. By

dx.doi.org/10.1021/cs5010536 | ACS Catal. 2014, 4, 3160–3168

comparison, oxygen-free hydrogenation such as styrene hydrogenation did not result in any phosphine oxidation.[34]

CONCLUSIONS

The organometallic synthesis of three different samples of Ru NPs combined with NMR and APXPS experiments allowed us to study the reactivity of ligand-capped ruthenium nanocatalysts in model FTS reactions. We compared the influence of two capping agents, a steric polymer (PVP) and a strongly coordinating diphosphine ligand (dppb), on Ru NPs with mean sizes 1.3, 1.9, and 3.1 nm.

We found that the surface modification by ligands, whether introduced as protecting agents during synthesis or afterward via ligand exchange, affected both selectivity and activity. APXPS results indicate that the dppb ligands undergo partial oxidation when exposed to catalytic conditions but nevertheless improved the activity of the Ru NPs in comparison with that of PVP-stabilized NPs. In particular, an increase in selectivity for C_2−C_4 alkanes and alkenes was observed under mild conditions of 150 °C and 3 bar of syngas. At this stage, one cannot decide if the effects observed are of a geometric or electronic nature. We believe, however, that these findings clearly demonstrate the importance of ligand effects in addition to the particle size effect on catalyst activity, in particular in the context of FTS, as this effect has the ability to tune the surface properties.

EXPERIMENTAL SECTION

(i) Ru-PVP and Ru-dppb NPs were prepared according to our previously described organometallic route.[30,31,36,57] Ru-hept-dppb NPs were obtained through a ligand-exchange procedure from preformed Ru-hept NPs.[36] All chemical operations were conducted using standard Schlenk tubes, Fischer−Porter bottle techniques, or in a glovebox under an argon atmosphere. Solvents were purified before use; THF (Sigma-Aldrich) was purified by distillation under an argon atmosphere and pentane (SDS) through filtration in the column of a purification apparatus (MBraun). Heptanol (Sigma-Aldrich) was deoxygenated by three freeze-pump cycles and stored in a flask on 4 Å molecular sieves (Sigma-Aldrich) under argon.

[Ru(cod)(cot)] was purchased from Nanomep Toulouse. CO and H_2 were purchased from Air liquide. CO (^{13}C, 99.14%) was purchased from Eurisotop. 1,4-Bis(diphenylphosphino)-butane (dppb) and polyvinylpyrrolidone (PVP) were purchased from Sigma-Aldrich. They were used without purification.

Synthesis of Ru-hept-dppb NPs. [Ru(cod)(cot)] (250 mg, 0.79 mmol) was introduced in a Fischer−Porter bottle and dissolved in heptanol (60 mL) degassed beforehand by three freeze-pump cycles. The resulting yellow solution was pressurized with 3 bar of H_2, and the solution was left to be stirred vigorously for 1 h. A black homogeneous solution was immediately formed. Excess H_2 was eliminated, and a solution of dppb (33.6 mg, 0.079 mmol) in THF (60 mL) was added. The reaction mixture was stirred for 14 h at r.t. After this period of time, the colloidal solution was concentrated by evaporation of the solvent mixture while being heated at 70 °C. Addition of 100 mL of pentane gave a black precipitate. The resulting precipitate was washed twice with pentane (50 mL) and dried overnight under vacuum. The mean size of the NPs was measured by TEM on a collection of at least 200 nanoparticles leading to a value of at 3.1(0.4) nm. Elemental analysis and ICP gave the following composition: 10.48% C, 1.5% H, 2.48% P, 69.6% Ru.

(ii) Catalytic reactions were conducted in Quick Pressure Valve (QPV) NMR sample tubes with a wall thickness of 5 mm and a volume of 2 mL closed with a Teflon needle valve as small-size reactors. The tube was filled at r.t. with Ru NPs as a dry powder. The mass of Ru NPs was determined to have from 0.02 to 0.05 mmol of Ru in the NMR tube. Prior to the reaction, the NPs were pretreated with H_2 (3 bar) for 12 h at 25 °C to prevent the presence of oxygen traces on their surface. The reaction was then conducted using a 1:1 molar mixture of ^{13}CO and H_2 with a total pressure of 3 bar. When required, the reactor was heated using an oil bath at a chosen temperature (120 or 150 °C) for 1−5 days. ^{1}H and ^{13}C gas-phase NMR spectra were recorded at the end of the reaction. The remaining gas phase was also analyzed by mass spectroscopy, which was limited to 100 g/mol as the maximal molar mass. To guarantee that the reaction did not yield heavier products, organic compounds were extracted from the NPs by adding anisole in the NMR tube to dissolve any present product and the collected solution was analyzed by gas chromatography. Heavier alkanes or alkenes were never detected following this procedure.

(iii) Solid samples were analyzed by WAXS, TEM, and solid state ^{13}C MAS NMR, and the gaseous products were studied by ^{13}C and ^{1}H gas NMR and mass spectrometry.

ICP and elemental analyses were performed at Institut des Sciences Analytiques, Département Service Central d'Analyse (CNRS) of Lyon.

Wide-angle X-ray scattering (WAXS) was performed at CEMES-CNRS. Samples were sealed in 1.5 mm diameter Lindemann glass capillaries. The samples were irradiated with graphite monochromatized molybdenum Kα (0.071069 nm) radiation, and the X-ray intensity scattered measurements were performed using a dedicated two-axis diffractometer. Radial distribution functions (RDFs) were obtained after Fourier transformation of the reduced intensity functions.

Solid state NMR (MAS NMR) analyses with and without ^{1}H−^{13}C cross-polarization (CP) were performed at the LCC on a Bruker Avance 400WB instrument equipped with a 2.5 mm probe with a sample rotation frequency of 12 kHz. Measurements were taken in a 2.5 mm ZrO_2 rotor.

Gas-phase NMR spectra were recorded on a Bruker AMX 500 NMR spectrometer at a magnetic field of 11.7 T. The corresponding resonance frequencies were 500.0 MHz for ^{1}H and 125.7 MHz for ^{13}C. Chemical shift calibration of the NMR spectra was performed using TMS as an external standard.

Mass chromatograms of gas samples were obtained in a LEYBOLD QX2000 quadrupole mass spectrometer.

TEM observations were performed at the Service Commun de Microscopie Electronique de l'Université Paul Sabatier (TEMSCAN) on a JEOL JEM 1011 CX-T electron microscope operating at 100 kV with a point resolution of 4.5 Å. TEM grids were prepared by drop-casting of the crude colloidal solution in THF on a holey carbon-coated copper grid.

(iv) The chemical state of the surface of the NPs was analyzed *in situ* by ambient-pressure X-ray photoelectron spectroscopy (APXPS), which allows exposure of the nanoparticles to gas up to a few torr. The experiments were conducted at beamline 9.3.2 of the Advanced Light Source in Berkeley, CA. For APXPS, NP powders were dissolved in dry and degassed THF in an Ar-filled glovebag and deposited on a

dx.doi.org/10.1021/cs5010536 | ACS Catal. 2014, 4, 3160−3168

gold foil by drop-casting. The sample was introduced into the beamline chamber under air-free conditions. A photon energy of 630 eV was used. Au 4f peaks were used to calibrate the binding energies of XPS peaks. The sample was moved very regularly under the beam to prevent beam damage: successive spectra taken at "old" and "fresh" positions did not show any significant difference.

■ ASSOCIATED CONTENT

Supporting Information

Figures, tables, complementary TEM and HRTEM images, WAXS data, APXPS and MAS NMR spectra, and the XPS fitting procedure. This material is available free of charge via the Internet at http://pubs.acs.org.

■ AUTHOR INFORMATION

Corresponding Authors

*E-mail: mbsalmeron@lbl.gov.

*E-mail: chaudret@insa-toulouse.fr.

Author Contributions

L.M.M.-P. and S.C. contributed equally to this work.

Funding

Notes

The authors declare no competing financial interest.

■ ACKNOWLEDGMENTS

We thank CNRS, University Paul Sabatier at Toulouse University, Institut des Sciences Appliquées at Toulouse (INSA), and V. Collière and L. Data for TEM facilities (TEMSCAN, UPS) and P. Lecante (CEMES, CNRS) for WAXS measurements, and C. Bijani and Y. Coppel for gas-phase and solid state NMR measurements. This work was supported by EU (ERC Advanced Grant, NANOSONWINGS 2009-246763). The *in situ* XPS part of this work was supported by the Director, Office of Science, Office of Basic Energy Sciences, Chemical Sciences, Geosciences, and Biosciences Division, under U.S. Department of Energy Contract DE-AC02-05CH11231. The Advanced Light Source is supported by the Director, Office of Science, Office of Basic Energy Sciences, of the U.S. Department of Energy under Contract DE-AC02-05CH11231.

■ REFERENCES

(1) James, O. O.; Chowdhury, B.; Mesubi, M. A.; Maity, S. *RSC Adv.* **2012**, *2*, 7347−7366.

(2) Dry, M. E.; Steynberg, A. P. In *Fischer−Tropsch Technology*; Elsevier: Amsterdam, 2004; Vol. *152*, pp 406−481.

(3) Maitlis, P. M.; Zanotti, V. *Chem. Commun.* **2009**, 1619−1634.

(4) Zhang, Q.; Kang, J.; Wang, Y. *ChemCatChem* **2010**, *2*, 1030−1058.

(5) Schulz, H. *Appl. Catal., A* **1999**, *186*, 3−12.

(6) De Smit, E.; Weckhuysen, B. M. *Chem. Soc. Rev.* **2008**, *37*, 2758−2781.

(7) Dalai, A. K.; Davis, B. H. *Appl. Catal., A* **2008**, *348*, 1−15.

(8) Tuxen, A.; Carenco, S.; Chintapalli, M.; Chuang, C.-H.; Escudero, C.; Pach, E.; Jiang, P.; Borondics, F.; Beberwyck, B.; Alivisatos, A. P.; Thornton, G.; Pong, W.-F.; Guo, J.; Perez, R.; Besenbacher, F.; Salmeron, M. *J. Am. Chem. Soc.* **2013**, *135*, 2273−2278.

(9) Vannice, M. *J. Catal.* **1975**, *37*, 462−473.

(10) Iglesia, E.; Soled, S.; Fiato, R.; Via, G. *J. Catal.* **1993**, *143*, 345−368.

(11) Kibby, C.; Jothimurugesan, K.; Das, T.; Lacheen, H. S.; Rea, T.; Saxton, R. J. *Catal. Today* **2013**, *215*, 131−141.

(12) Kang, J.; Zhang, S.; Zhang, Q.; Wang, Y. *Angew. Chem., Int. Ed.* **2009**, *48*, 2565−2568.

(13) Xiong, K.; Li, J.; Liew, K.; Zhan, X. *Appl. Catal., A* **2010**, *389*, 173−178.

(14) Quek, X.-Y.; Guan, Y.; van Santen, R. a.; Hensen, E. J. M. *ChemCatChem* **2011**, *3*, 1735−1738.

(15) González Carballo, J. M.; Finocchio, E.; García, S.; Rojas, S.; Ojeda, M.; Busca, G.; Fierro, J. L. G. *Catal. Sci. Technol.* **2011**, *1*, 1013−1023.

(16) Yin, A.-X.; Liu, W.-C.; Ke, J.; Zhu, W.; Gu, J.; Zhang, Y.-W.; Yan, C.-H. *J. Am. Chem. Soc.* **2012**, *134*, 20479−20489.

(17) Wang, C.; Zhao, H.; Wang, H.; Liu, L.; Xiao, C.; Ma, D. *Catal. Today* **2012**, *183*, 143−153.

(18) Lignier, P.; Bellabarba, R.; Tooze, R. P.; Su, Z.; Landon, P.; Ménard, H.; Zhou, W. *Cryst. Growth Des.* **2012**, *12*, 939−942.

(19) Carballo, J. M. G.; Finocchio, E.; García-Rodriguez, S.; Ojeda, M.; Fierro, J. L. G.; Busca, G.; Rojas, S. *Catal. Today* **2013**, *214*, 2−11.

(20) Carballo, J. M. G.; Yang, J.; Holmen, A.; García-Rodríguez, S.; Rojas, S.; Ojeda, M.; Fierro, J. L. G. *J. Catal.* **2011**, *284*, 102−108.

(21) Joo, S. H.; Park, J. Y.; Renzas, J. R.; Butcher, D. R.; Huang, W.; Somorjai, G. A. *Nano Lett.* **2010**, *10*, 2709−2713.

(22) Gual, A.; Godard, C.; Castillón, S.; Curulla-Ferré, D.; Claver, C. *Catal. Today* **2012**, *183*, 154−171.

(23) Zhang, Y.; Grass, M. E.; Kuhn, J. N.; Tao, F.; Habas, S. E.; Huang, W.; Yang, P.; Somorjai, G. A. *J. Am. Chem. Soc.* **2008**, *130*, 5868−5869.

(24) Xia, Y.; Xiong, Y.; Lim, B.; Skrabalak, S. E. *Angew. Chem., Int. Ed.* **2009**, *48*, 60−103.

(25) Tao, A. R.; Habas, S.; Yang, P. *Small* **2008**, *4*, 310−325.

(26) Lara, P.; Philippot, K.; Chaudret, B. *ChemCatChem* **2013**, *5*, 28−45.

(27) Quek, X.-Y.; Pestman, R.; van Santen, R. A.; Hensen, E. J. M. *ChemCatChem* **2013**, *5*, 3148−3155.

(28) Iglesia, E.; Soled, S.; Fiato, R. *J. Catal.* **1992**, *224*, 212−224.

(29) Hibbitts, D. D.; Loveless, B. T.; Neurock, M.; Iglesia, E. *Angew. Chem., Int. Ed.* **2013**, *52*, 12273−12278.

(30) Pan, C.; Pelzer, K.; Philippot, K.; Chaudret, B.; Dassenoy, F.; Lecante, P.; Casanove, M. J. *J. Am. Chem. Soc.* **2001**, *123*, 7584−7593.

(31) García-Antón, J.; Axet, M. R.; Jansat, S.; Philippot, K.; Chaudret, B.; Pery, T.; Buntkowsky, G.; Limbach, H.-H. *Angew. Chem., Int. Ed.* **2008**, *47*, 2074−2078.

(32) Nijs, H. H.; Jacobs, P. A.; Uytterhoeven, J. B. *J. Chem. Soc., Chem. Commun.* **1979**, 1095−1096.

(33) Kinayyigit, S.; Lara, P.; Lecante, P.; Philippot, K.; Chaudret, B. *Nanoscale* **2014**, *6*, 539−546.

(34) Novio, F.; Monahan, D.; Coppel, Y.; Antorrena, G.; Lecante, P.; Philippot, K.; Chaudret, B. *Chemistry* **2014**, *20*, 1287−1297.

(35) Novio, F.; Philippot, K.; Chaudret, B. *Catal. Lett.* **2010**, *140*, 1−7.

(36) Pelzer, K.; Philippot, K.; Chaudret, B. *Z. Phys. Chem.* **2003**, *217*, 1539−1548.

(37) Lara, P.; Rivada-Wheelaghan, O.; Conejero, S.; Poteau, R.; Philippot, K.; Chaudret, B. *Angew. Chem., Int. Ed.* **2011**, *50*, 12080−12084.

(38) Van Der Laan, G. P.; Beenackers, A. A. C. M. *Catal. Rev.* **1999**, *41*, 255−318.

(39) González-Gálvez, D.; Nolis, P.; Philippot, K.; Chaudret, B.; van Leeuwen, P. W. N. M. *ACS Catal.* **2012**, *2*, 317−321.

(40) Tschan, M. J.-L.; Diebolt, O.; van Leeuwen, P. W. N. M. *Top. Catal.* **2014**, *57*, 1054−1065.

(41) Grass, M. E.; Karlsson, P. G.; Aksoy, F.; Lundqvist, M.; Wannberg, B.; Mun, B. S.; Hussain, Z.; Liu, Z. *Rev. Sci. Instrum.* **2010**, *81*, 053106−053107.

(42) Starr, D. E.; Liu, Z.; Hävecker, M.; Knop-Gericke, A.; Bluhm, H. *Chem. Soc. Rev.* **2013**, *42*, 5833−5857.

(43) Salmeron, M.; Schlogl, R. *Surf. Sci. Rep.* **2008**, *63*, 169−199.

(44) Hävecker, M.; Mayer, R. W.; Knop-Gericke, A.; Bluhm, H.; Kleimenov, E.; Liskowski, A.; Su, D.; Follath, R.; Requejo, F. G.;

Ogletree, D. F.; Salmeron, M.; Lopez-Sanchez, J. A.; Bartley, J. K.; Hutchings, G. J.; Schlögl, R. *J. Phys. Chem. B* **2003**, *107*, 4587−4596.
(45) Halevi, B.; Peterson, E. J.; DeLaRiva, A.; Jeroro, E.; Lebarbier, V. M.; Wang, Y.; Vohs, J. M.; Kiefer, B.; Kunkes, E.; Havecker, M.; Behrens, M.; Schlögl, R.; Datye, A. K. *J. Phys. Chem. C* **2010**, *114*, 17181−17190.
(46) Halevi, B.; Peterson, E. J.; Roy, A.; DeLariva, A.; Jeroro, E.; Gao, F.; Wang, Y.; Vohs, J. M.; Kiefer, B.; Kunkes, E.; Hävecker, M.; Behrens, M.; Schlögl, R.; Datye, A. K. *J. Catal.* **2012**, *291*, 44−54.
(47) Piccinin, S.; Zafeiratos, S.; Stampfl, C.; Hansen, T. W.; Hävecker, M.; Teschner, D.; Bukhtiyarov, V. I.; Girgsdies, F.; Knop-Gericke, A.; Schlögl, R.; Scheffler, M. *Phys. Rev. Lett.* **2010**, *104*, 035503−035504.
(48) Carenco, S.; Tuxen, A.; Chintapalli, M.; Pach, E.; Escudero, C.; Ewers, T. D.; Jiang, P.; Borondics, F.; Thornton, G.; Alivisatos, A. P.; Bluhm, H.; Guo, J.; Salmeron, M. *J. Phys. Chem. C* **2013**, *117*, 6259−6266.
(49) Arrigo, R.; Hävecker, M.; Schuster, M. E.; Ranjan, C.; Stotz, E.; Knop-Gericke, A.; Schlögl, R. *Angew. Chem., Int. Ed.* **2013**, *52*, 11660−11664.
(50) Starr, D. E.; Bluhm, H. *Surf. Sci.* **2013**, *608*, 241−248.
(51) Qadir, K.; Kim, S. M.; Seo, H.; Mun, B. S.; Akgul, F. A.; Liu, Z.; Park, J. Y. *J. Phys. Chem. C* **2013**, *117*, 13108−13113.
(52) Crotti, C.; Farnetti, E.; Celestino, T.; Stener, M.; Fontana, S. *Organometallics* **2004**, *23*, 5219−5225.
(53) Shin, J.; Waheed, A.; Winkenwerder, W. A.; Kim, H.-W.; Agapiou, K.; Jones, R. A.; Hwang, G. S.; Ekerdt, J. G. *Thin Solid Films* **2007**, *515*, 5298−5307.
(54) Qadir, K.; Joo, S. H.; Mun, B. S.; Butcher, D. R.; Renzas, J. R.; Aksoy, F.; Liu, Z.; Somorjai, G. A.; Park, J. Y. *Nano Lett.* **2012**, *12*, 5761−5768.
(55) Shetty, S.; van Santen, R. A. *Catal. Today* **2011**, *171*, 168−173.
(56) Loveless, B. T.; Buda, C.; Neurock, M.; Iglesia, E. *J. Am. Chem. Soc.* **2013**, *135*, 6107−6121.
(57) It was necessary to heat slightly the solution of PVP in THF to solubilize it completely.